

Heat Transfer Analysis of Zeotropic Refrigerants with Falling Film Evaporation on Plain Tubes

Ching-Hung Chang* and Liang-Han Chien**

Keywords : zeotropic, falling film evaporation, heat transfer coefficient, refrigerant

ABSTRACT

This study investigated mixtures of the refrigerants R-152a and R-245fa with various blending ratios and saturation temperatures in falling film evaporation heat transfer. It explored the respective heat transfer properties of R-152a/R-245fa at blending ratios of 0.75/0.25 and 0.25/0.75. For the falling film evaporation, a plain tube was placed horizontally in a chamber with saturated temperatures of 10°C and 20°C. The test results showed that the heat transfer performance variation is not linearly proportional to the blending ratio of the refrigerant. The heat transfer distribution band of the R-152/R-245fa ratio = 0.25/0.75 mixed refrigerants was wider than that of the 0.75/0.25 mixed refrigerant. A possible reason for this was that the blending ratios caused differences in temperature glide. The heat transfer performance of the mixture was higher than pure R-245fa. The top tube was effectively increased by 0.39–0.55 and the center tube was effectively increased by 0.57–0.78. The boiling heat transfer performance of both mixtures are less than the ideal heat transfer coefficient calculated from the boiling curve of the pure R-152a and R-245fa. Instead of performance degradation, the falling film evaporative heat transfer of the R-152a/R-245fa mixture is greater than the ideal value at 0.25 mass concentration of R-152a.

INTRODUCTION

Air conditioning improves people's quality of life by allowing their daily activities to go unaffected by external environmental changes. Refrigerant are indispensable fluids in refrigeration system. In the early days of refrigeration, CFCs were widely used, and the

most common refrigerants were R-22, R-11, R-12. In 1987, the United Nations invited 26 countries to a meeting in Canada to discuss how to mitigate destruction of the global environment. Guidelines were proposed to all countries, and the participating countries signed "The Montreal Protocol on Substances that Deplete the Ozone Layer".

The guidelines mainly concerned restricting the use of ozone-depleting substances and specify limits on the use of halogen-containing CFCs. This protocol came into effect on January 1, 1989, with the hope of completely eliminating CFC refrigerants by 2040 (included R-11 and R-12). With the use of HFCs as alternatives to ozone-depleting substances, their role in warming the atmosphere became a greater concern. The Kigali Amendment to the Montreal Protocol entered into force on 1 January 2019, following ratification by 65 countries. Under the Amendment, all countries will gradually phase down HFCs by more than 80 percent over the next 30 years and replace them with more environmentally friendly alternatives. The UN Environment Program announced the entry into force, and noted that it will help reduce the production and consumption of hydrofluorocarbons (HFCs), potent greenhouse gases (GHGs), and thus to avoid global warming by up to 0.4°C this century.

To develop new alternative refrigerant, factors such as a stable material state, safe operation, minimal environmental damage, high system compatibility, and easy access must be considered. The development of refrigerant has expanded to the mixed refrigerants. In refrigerant classifications, code 4 represents a mixed refrigerant. Two types of mixed refrigerants exist: azeotropes and zeotropics. When the two types are mixed at a certain ratio, they can no longer be separated through the redistilled method. The azeotrope acts as a new refrigerant substance with a constant boiling point under a specific temperature and pressure (e.g., the commercial refrigerants R-500-series). For zeotropics, temperature changes during the phase change of a mixture of two refrigerants are termed temperature glide. The commercial refrigerants R400-series are zeotropics. Table 1 presents a variety of new refrigerant that were developed to replace CFC refrigerant. Many scholars have studied refrigerant mixtures. Stralen and Sluyter (1969), Stralen (1970) found that the pool boiling of 1-butanol / water and 2-butanone / water

Paper Received Nov, 2019. Revised February, 2020, Accepted April, 2020, Author for Correspondence: Ching-Hung Chang

* Graduate Student, Department of Energy and Refrigerating Air-Conditioning Engineering, National Taipei University of Technology, Taipei, 10608, ROC.

** Associate Professor, Department of Energy and Refrigerating Air-Conditioning Engineering, National Taipei University of Technology, Taipei, 10608, ROC.

blending ratio will affect critical heat flux (CHF). Jung et al. (2003) conducted experimental research on pool boiling heat transfer of R-32, R-125, R-134a and binary mixture refrigerant on a horizontal smooth tube. The heat transfer coefficient of the zeotropic mixtures of HFC32/HFC134a, HFC125/HFC134a, and HFC32/HFC125/HFC134a showed as much as 40% reduction from the ideal values Sarbu (2014) proposed that mixture refrigerants can effectively reduce GWP and increase the efficiency of refrigeration, and as the main substitute for CFC and HCFC refrigerants. Dang et al. (2017) found an important advantage of the azeotropic refrigerant is that it can effectively avoid drying out.

Many studies have investigated falling film evaporation. Moeykens and Pate (1994), Moeykens et al. (1996) conducted a series of falling film evaporation tests that use a single horizontal tube and tube array structure using R-22, R-123, and R-134a. Chang and Chiou (1999) used R-141b to test a 3 × 5 plain tube bundle in falling film evaporation tests, and discovered that the heat transfer could be enhanced by the addition of a liquid collection tray under each tube. Chien and Cheng (2006) developed a superposition model for the falling film evaporation of refrigerants in horizontal plain tubes. Ribatski and Jacobi (2005) further discussed falling film evaporation in horizontal tubes. They concluded that some basic mechanisms responsible for heat transfer remained unclear. The effect and occurrence of nucleate boiling are confused by heat flux, flowrate, fluid properties. Among some models focusing on the prediction of heat transfer coefficients have been propounded; however, none have included nucleate boiling, vapor-phase shear stress, or interfacial moire effects. Experimental data for four different refrigerants, R-22, R-134a, R-141b, and R-123 Moeykens and Pate (1994) and Moeykens et al. (1996), Chang and Chiou (1999), Fujita and Tsutsui (1998), Fujita et al (1995 a,b), Moeykens and Pate (1995, 1996), Moeykens et al (1995) have predicted uncertainty of -20% to +25%. Chien and Cheng (2006) assumed that the general heat transfer coefficient is the sum of convection and nucleate boiling, where convection is an empirical formula, that based on falling film evaporation on a vertical plate.

Under the same chiller refrigeration capacity, the falling film evaporator uses less refrigerants than a flooded evaporator. Fujita and Tsutsui (1998), Fujita et al. (1995 a,b), performed a falling film evaporation test using R-11 with a set of plain tubes with diameters of 25 mm. They observed the falling film phenomenon and differentiated it into discontinuous liquid-drop, cylindrical, sheet forms and disordered cylindrical. According to a turbulence analysis, they proposed an empirical formula that using data on R-11 to predict the heat transfer coefficient within a range of ± 20%. Roques and Thome(2007) used R-134a (at 5°C) to perform a falling film evaporation test on four types of tube (Gewa-B, Turbo-BII-HP, High-flux, and plain)

under three different tube spacings and nominal heat flux. Flow patterns between tubes were determined, but no notable differences were observed in the heat transfer coefficients of the different flow patterns in each region. Fernández-Seara and Pardiñas (2014) presented a comprehensive review on falling film evaporation and concluded that the heat transfer coefficients of enhanced boiling tubes decrease or remain almost constant with heat flux. Ji et al. (2016) and Zhao et al. (2017, 2018) found that the effect of vapor flow velocity is complex. In general, the cross vapor notably enhanced heat transfer at higher film flow rates or at lower heat fluxes. Jin et al. (2019) proposed falling film evaporation correlations for fully and partially wetted regimes. Chien et al. (2019) investigated the effect of oil in R-245fa/oil mixture, and found that the heat transfer coefficient increases with increasing oil concentration in most tests.

Table 1. Common Refrigerants list

R-No	Type	Material	ODP	GWP	Replace	Class
R-11	CFC	pure	1	3400	R-123	A1
R-12	CFC	pure	1	10900	R-134a	A1
R-22	HCFC	pure	0.055	1780	R-410a	A1
R-32	HFC	pure	0	675		A2
R-134a	HFC	pure	0	1430	R-1234yf	A1
R-152a	HFC	pure	0	140	---	A2
R-123	HCFC	pure	0.012	120		B1
R-1234yf	HFO	pure	0	4		A2L
R-290	HC	pure	0	6.3		A3
R-245fa	HCFC	pure	0	1030	---	B1
R-410a	HFC	mixtures	0	1924	---	A1
R-407C	HFC	mixtures	0	1774	---	A1
R-507c	HFC	mixtures	0	0.847	R-502	A1

Experiment setup

Apparatus

In this study, the mixed refrigerant was used as the working fluid. In the small-sized chamber, a drip tube served as the fluid distributor, and three copper tubes with built-in heaters were made to simulate the chiller water pipes. In order to maintain the temperature inside the chamber, a set of spiral type cooler were arranged above the chamber to simulate the falling film evaporator phenomenon experimentally. This experimental device is shown in Fig.1

Fig.1 presents the experimental setup of this study, where (a) is a constant-temperature bath, (b) is a flow meter, (c) is a data miner, (d) is a pressure transmitter, (e) is a micro gear pump, (f) is a window, (g) is a filter, (h) is a cooling coil, (i) is a test tube, and (j) is an experimental chamber.

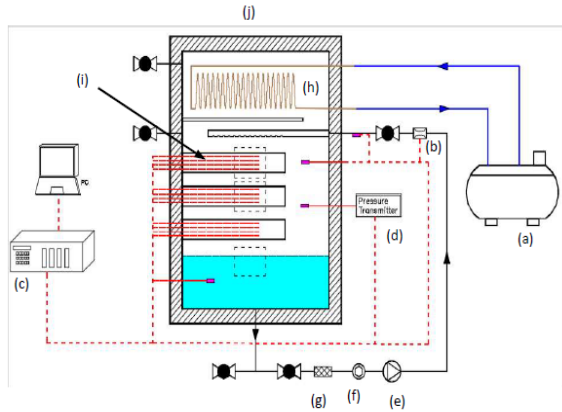


Fig. 1. Schematic of the test cell

In this study, the falling film evaporator was operated using three round tubes. Fig.3 illustrates the arrangement of the tubes. The heat transfer performance was measured. The experimental apparatus was a closed system with components connected by a closed chamber and gear pump that had a copper pipe with an outside diameter of 19 mm. The gear pump was placed under the chamber, and the flow meter was installed at the chamber inlet of the refrigerant tube. Temperature and pressure sensors were installed in the chamber. Furthermore, a temperature sensor was installed on the inlet pipe inserted into the chamber to measure the inlet refrigerant temperature. A cooling coil was placed above the chamber to cool it and ensure a saturated state was maintained inside. Moreover, a drip trap plate was placed under the cooling coil to guide the condensed liquid refrigerant to flow to the bottom of the chamber for storage without dripping directly onto the heating tube underneath.

A drip tube that featured an outside diameter (d_o) of 6.35 mm and 15 drip holes with diameters of 1.0 mm was placed under a guide plate to simulate the falling film phenomenon. Three copper test tubes with outside diameters (d_o) of 19 mm were placed directly under the drip tube, and a 200 kW heating rod was placed in the copper tube to simulate the heating of the evaporator's inner tubes (Fig.2). Moreover, a repair valve was installed above the chamber to fill it with refrigerants as well as for system vacuuming, and another repair valve was installed below the chamber to discharge liquid refrigerants. To obtain the surface temperature of the test tubes, four holes surrounding each tube were drilled with diameters of 0.5 mm and depths (T_L) of 50 mm; in each hole, a stainless sheath thermocouple transmitter was inserted. The temperature measurement signal was connected to the datalogger for temperature measurements.

Furthermore, the cooling coil was connected to a bath with a constant temperature (to maintain the temperature inside the chamber) using a piping method. The fluid inside bath was ethylene glycol solution.

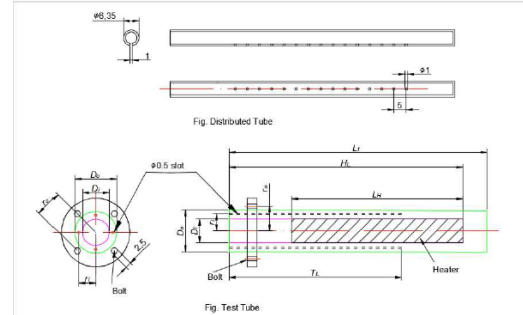


Fig. 2 the diagram of test tube and fluid distributor

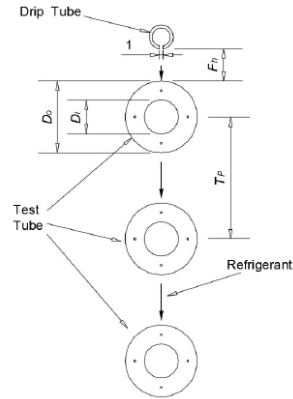


Fig. 3 Arrangement of test tube and fluid distributor

Scope of the tests

In this study, tests were conducted to determine the heat transfer characteristics of two types of refrigerants: pure and mixed. The pure refrigerants were R-152a and R-245fa, and the mixed refrigerants were R-152a mixed with R-245fa at ratios of 0.25/0.75 and 0.75/0.25.

Table 3 lists the refrigerants' properties. The liquid refrigerants flow rates were 240 and 300 mL·min⁻¹, the chamber saturation temperatures were 10°C, 20°C, and the unit heating capacity was from 10 to 50 kW·m⁻²; data were recorded at intervals of 5 kW·m⁻². Table 2 presents a detailed list of all the tests.

Test procedures

Before the installation, all the test tube surfaces and test chambers were cleaned with alcohol. System stand and station pressure tests were required after installation to ensure that the test system was free of leaks.

Table 2. Test Parameter

working fluid	R-245fa R-152a 0.25 R-152a : 0.75 R-245fa 0.75 R-152a : 0.25 R-245fa
Saturate Temp. (°C)	10°C · 20°C
test tube	plain tube
d_o (mm)	19
Feeder	Ø 1.0 mm of hole · 15 holes
Heat flux, q'' (kW m ⁻²)	10 ~50
Install Level pitch of test Tube, F_p (mm)	9.5

Interval of Test Tube, T_p , (mm) | 28.5 mm

Table 3. Thermal properties of refrigerants

(a) R-245fa, R-152a refrigerants

	R-245fa		R-152a	
	10	20	10	20
T_{sat} (°C)	10	20	10	20
P_{sat} (MPa)	0.08242	0.12306	0.37276	0.5129
P_c (MPa)	3.651	3.651	4.5168	4.5168
ρ_{liq} (kg m ⁻³)	1378.3	1351.9	936.07	911.97
ρ_{vap} (kg m ⁻³)	4.871	7.1121	11.651	15.909
h_g (kJ kg ⁻¹)	212.73	225.68	217.19	234.77
h_f (kJ kg ⁻¹)	412.22	419.72	513.78	520.09
Cp_{liq} (kJ kg ⁻¹ K ⁻¹)	1.2824	1.3048	1.7342	1.7765
Cp_{vap} (kJ kg ⁻¹ K ⁻¹)	0.85969	0.88844	1.1517	1.2173
μ_{liq} (μpa-s)	496.2	429.49	194.28	172.76
σ (N m ⁻¹)	15.571	14.266	11.741	10.378
Molar mass (kg kmol ⁻¹)	134.05	134.05	66.051	66.051

(b) R-152a / R-245fa mixed refrigerants

	R-152a / R-245fa (0.25 / 0.75)		R-152a / R-245fa (0.75 / 0.25)	
	10	20	10	20
T_{sat} (°C)	10	20	10	20
Liquid Phase P_{sat} (MPa)	0.21207	0.29491	0.33349	0.45955
Vapor Phase P_{sat} (MPa)	0.12517	0.18523	0.27006	0.3828
P_c (MPa)	4.1502	4.1502	4.4518	4.4518
ρ_{liq} (kg m ⁻³)	1226.3	1200.1	1014.5	989.5
ρ_{vap} (kg m ⁻³)	5.937	8.6141	9.4179	13.196
h_g (kJ kg ⁻¹)	213.83	227.92	216.06	232.48
h_f (kJ kg ⁻¹)	435.68	443.14	487.74	494.54
Cp_{liq} (kJ kg ⁻¹ K ⁻¹)	1.3934	1.4206	1.6199	1.657
Cp_{vap} (kJ kg ⁻¹ K ⁻¹)	0.91417	0.94851	1.0561	1.1091
μ_{liq} (μpa-s)	334.38	293.54	218.36	193.76
μ_{vap} (μpa-s)	10.037	10.407	9.8593	10.221
Pr_{liq} (cm ² s ⁻¹)	4.863	4.5261	3.476	3.2895
Pr_{vap} (cm ² s ⁻¹)	0.76894	0.76491	0.81761	0.81933
σ_{liq} (N m ⁻¹)	13.886	12.556	12.215	10.861
σ_{vap} (N m ⁻¹)	15.062	13.689	13.062	11.622
Molar mass (kg kmol ⁻¹)	106.61	106.61	75.644	75.644

First, all valves in the system pipeline were opened and connected to an air compressor machine, which was activated to pressurize the system to 2.0 kg·cm⁻². The repair valve was turned off to inspect and note the value stated on the pressure gauge. Subsequently, all screw-threaded splicing points and locking points were tested with foam to check for leaks. The valve was immediately tightened if any leaks were found. Next, the system was re-pressurized to 2.0 kg·cm⁻², the repair valve was turned off, and the value on the pressure gauge was noted. The system was allowed to cool for 2 hours, and then the value on the pressure gauge was again noted to determine whether

the pressure decreased. If pressure decreased, it would be necessary to perform leak detection again; otherwise, the system pressure can be released and the repair valve connected to a vacuum pump. The repair valve was opened and the vacuum pump was activated to perform vacuum pumping to 10⁻³ Torr for 1 h. Next, the repair valve and vacuum pump were closed and a system pressure station test was performed using a data collector. After the system had operated continuously for 4 hours, it was considered airtight and leak-free, and thus, it could be filled with refrigerants, which was in liquid form. Before filling commenced, weighting and recording were performed. During the filling process, the constant-temperature bath had to be open, and the temperature was set 5°C lower than room temperature to lower the pressure in the chamber and accelerate the filling process. Furthermore, a hydraulic pump was activated to increase the speed at which the chamber was filled with refrigerants. The liquid level could be observed through the chamber window. The filling process was stopped when the amount of refrigerants reached the upper edge of the third test tube.

When test began, the electric heater was adjusted to its maximum output, and start up the water pump, the flow of cooling water and temperature of the bath were adjusted to maintain the chamber temperature at the desired system temperature for at least 1 hour, make the test system to reach steady situation. Under a fixed heat input, the pump drive controller was used to regulate the refrigerant flow to ensure a steady flow state. Data were recorded after the system temperature had remained stable for at least 5 min.

To reduce the electric heater input, the input alternating voltage and current were gradually reduced. After each heat input adjustment, the system temperature was stabilized for at least 5 min before the data were recorded. The abovementioned steps were repeated for the different refrigerants and flowrates.

Data reduction

By dividing the heat flux (q'') by the wall superheat, the heat transfer coefficient (h) was determined by Eq. (1). The temperature difference is $\Delta T_{ws} = (T_w - T_s)$.

$$h = \frac{q''}{\Delta T_{ws}} \tag{1}$$

Here, q'' and h were calculated based on the envelop area, which was calculated by multiplying the heating length by the tube external circumference ($2\pi r_o L_h$). The input power (W) of the electric heater was calculated by operating voltage (V) multiply the electric heater current (I). The electric heater voltage (V) was measured that use a data acquisition system to collect, and the electric current (I) of each tube was measured using a calibrated digital meter.

The saturation temperature (T_s) was the average values of two copper-constantan sheathed thermocouples placed on the top of vapor and bottom

of the boiling liquid of flask. The cell temperature must be maintained within $\pm 0.2^\circ\text{C}$ during the test. The tube surface temperature (T_w) was calculated that use the average temperature (T_m) of four thermocouples on four sides of the tube brink, as shown in Eq. (2). presents the thermocouple configuration, where r_i is the distance of the thermocouple from the tube center, r_o is the external radius of the tube, L_h is the heating length, the thermal conductivity of copper k is $390 \text{ W m}^{-1}\text{K}^{-1}$.

$$T_w = T_m - \frac{Q \cdot \ln \frac{r_o}{r_i}}{2\pi k L_h} \quad (2)$$

Changes in mass flow rate from the top tube to the bottom tube were calculated using Eq. (4). The top, center, and bottom tubes were numbered $i = 1, 2,$ and 3 . When the inlet fluid temperature ($T_{in,i}$) of the i^{th} tube was less than the saturation temperature, the heat transfer coefficient was calculated by Eq. (3) to correct the sensible heat produced from subcooling ($T_s - T_{in,i}$). In this study, $(T_s - T_{in,i}) < 0.6^\circ\text{C}$.

$$h_i = \frac{q'' - \frac{\dot{m}_i C_p (T_s - T_{in,i})}{A_t}}{T_w - T_s} \quad (3)$$

In Eq. (3), the mass flow rate in the i^{th} row (\dot{m}_i) was calculated using Eq. (4):

$$\dot{m}_i = \dot{m}_{i-1} - \frac{q''_{i-1} \cdot A_t - \dot{m}_{i-1} \cdot C_p (T_s - T_{in,i})}{h_{fg}} \quad (4)$$

Except for the first tube ($T_{in,i} = T_{in}$), the inlet fluid temperature in the i^{th} row ($T_{in,i}$) was calculated using Eq. (5):

$$T_{in,i} = T_{in,i-1} + \frac{q''_{i-1} A_t}{\dot{m}_{i-1} C_p} \quad (5)$$

In the second term on the right side of Eq. (5) is the temperature rose when subcooled fluid passed through the previous tube. However, if the second item is greater than $(T_s - T_{in,i-1})$, it is set to $T_{in,i} = T_s$. In addition, $(T_s - T_{in,i}) = 0$ for most tests of the center and bottom tubes ($i = 2$ and 3).

The film's Reynolds number was calculated using Eq. (6)

$$Re_f = \frac{4 \cdot \Gamma}{\mu} \quad (6)$$

where Γ is the mass flow rate per unit length. Note that the fluid was only distributed over length L_h of the heating portion, and only half of the mass flow rate (kg s^{-1}) flowed on each side of the tubes' perimeter. Therefore, Γ was derived using Eq.(7).

$$\Gamma = \dot{m} / 2L_h \quad (7)$$

The working fluids were R-245fa, R-152a, and mixed refrigerants of R-152a/R-245fa (0.25/0.75) and R-152a/R-245fa (0.75/0.25). Table 3 lists the fluid properties at $5\text{--}20^\circ\text{C}$.

Experimental uncertainty

All thermocouples were connected to an Agilent 34970A data logging system. The reproducibility of the thermocouples was checked prior to tests and calibrated over a temperature range of $0\text{--}40^\circ\text{C}$ using a Galileo thermometer with a 0.05 K precision scale. The thermocouple had an uncertainty of $\pm 0.1^\circ\text{C}$ (between 0°C and 40°C) compared with a standard thermometer.

Because uncertainty was revealed in the heat flux and heat transfer coefficient measurements, this study proposed the uncertainty (R) of all measuring devices and derived $w(R)$ using Eq. (8).

$$\frac{w(R)}{R} = \left[\left(\frac{\partial R}{\partial x_1} \cdot \frac{w(x_1)}{R} \right)^2 + \left(\frac{\partial R}{\partial x_2} \cdot \frac{w(x_2)}{R} \right)^2 + \dots \right]^{1/2} \quad (8)$$

where R is an independent variable function of $x_1, x_2, x_3, \dots, x_n$, and $w(x_1)$ and $w(x_2)$ uncertainty are variables of $x_1, x_2, \dots,$ and x_n .

From Eq. (8), the uncertainty of the heat transfer coefficient was derived that use Eq. (9).

$$\frac{w(h)}{h} = \left[\left(1 \cdot \frac{w(q'')}{q''} \right)^2 + \left(-1 \cdot \frac{w(T_w - T_s)}{(T_w - T_s)} \right)^2 \right]^{1/2} \quad (9)$$

In addition, the uncertainties of the wall temperature (T_w), saturation temperature (T_s), and heat flux (q'') were calculated using Eq. (9). The heat flux distribution was tested using a numerical simulation, which resulted in heat loss from two unheated portions at the tube ends through natural convection, as well as an uneven heat flux distribution from the electric heater. The findings indicated that the heat flux uncertainties were approximately 5% and 8% at 10 and 30 kW m^{-2} , respectively. The uncertainty of the heat transfer coefficient increased when the wall superheat decreased. For the plain tubes, the maximum uncertainty of the heat transfer coefficient was 11.8%.

RESPONSE RESULTS AND DISCUSSIONS

This study explored the heat transfer properties of mixed refrigerants and compared them with pure refrigerant. The heat transfer coefficient measurements of R-152a and R-245fa were performed.

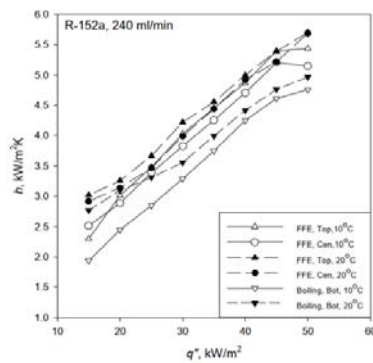
The saturated liquid refrigerant flowed down through the fluid distribution tube, the flow field of which was a laminar flow. The refrigerant continued to drip because of gravity and cover the test tube surface. Such dripping can affect the fluid's physical properties because of fluid temperature, surface tension, viscosity, thermal diffusivity, and density. Subsequently, a heat transfer test was conducted on the fluid after a heat source was added to the test tube. The surface

roughness of the test tube and physical properties of the refrigerants can affect its heat transfer performance. The heat transfer for falling film evaporation was performed when the refrigerants was exposed to the heat of the test tube.

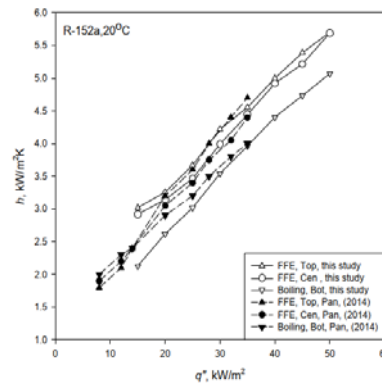
Falling film heat transfer of a plain tube: R-152a

Fig. 4 (a) presents the experimental results of a plain tube in R-152a refrigerants with evaporation temperatures of 10°C and 20°C and heat fluxes of 10–50 kW m⁻²K⁻¹, experimental observations indicated that under the same evaporation temperature, as the heat flux increased, falling film evaporation on the tube surface also increased, leading to increased heat transfer coefficient. Heat transfer coefficient at the top tube was higher than that at the center tube because the top tube received the dripped refrigerants first and had a sufficient amount of refrigerants, and furthermore, the liquid film on the tube surface was thicker, which meant that the surface was not prone to dryness. By contrast, the thickness of the center tube was reduced because of falling film evaporation on the surface of the top tube; thus, the heat transfer performance was slightly lower than that of the top tube. By comparing the heat transfer performance under different flow rates, this study found that higher flow rates can result in greater heat transfer. Fig. 4 (b) compares the overall experimental data of pure R152a in this study with that of Pan (2014) at an evaporation temperature 20°C. The data in Fig. 4(b) showed that the heat transfer coefficients in these two studies are in good agreement.

The falling film evaporation mechanism was related flow rate. When the flow rate was large under the same evaporation temperature, a thicker liquid film caused the film evaporation mechanism to be suppressed and the heat transfer coefficient to become smaller. The larger the flow rate, the less likely the test tube surface was to dry out even if it evaporated; here, the film Reynolds number had little effect on the heat transfer performance of falling film evaporation. Moreover, the film evaporation performance was affected by the thickness of the film.



(a) falling film and boiling for experiment with R-152a

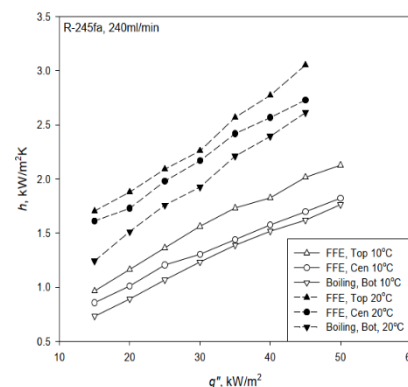


(b) comparison of this study with Pan study with R-152a

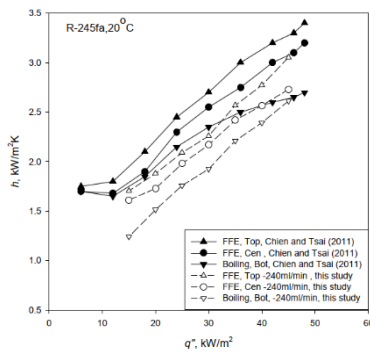
Fig. 4 (a) Comparison of falling film methods and boiling at various temperatures in R-152a; (b) comparison of this study with Pan study in R-152a

Falling film heat transfer of a plain tube: R-245fa

Fig. 5 (a) present experimental results of the heat transfer performance of the top and center tubes with R-245a under evaporation temperatures of 10°C and 20°C and heat fluxes of 15–50 kW m⁻²K⁻¹. The findings indicated that under the same evaporation temperature, the heat flux increased when the flow rate increased. Furthermore, the heat transfer coefficient of the top tube was notably higher than that of the center tube. The heat transfer coefficient at a saturation temperature of 20°C was higher than that at 10°C. This maybe because that the surface tension decreases with increasing temperature, resulting in a better evaporation effect. Fig. 5 (b) compares the results of this study with the study of Chien. and Tsai.(2011), which was conducted on a similar test system with additional subcooling devices. The heat transfer of this experiment was slightly lower but the heat transfer trend was consistent. This was because the subcooling devices help improved the heat transfer performance.



(a) falling film and boiling for experiment with R-245fa

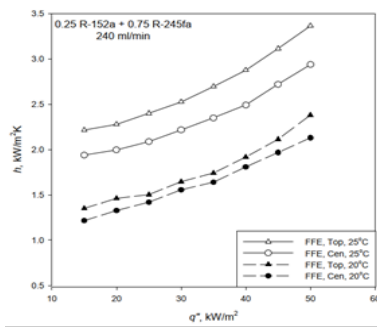


(b) comparison of this study with Pan study with with R-245fa

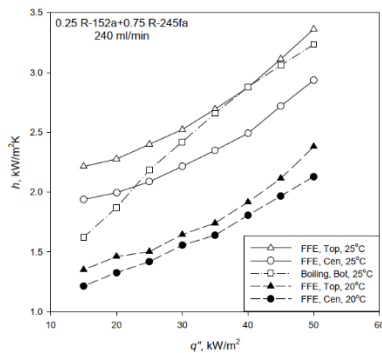
Fig. 5 (a) Comparison of falling film methods and boiling at various temperatures in R-245fa; (b) comparison of this study with Tsai study in R-245fa.

Falling film on plain tubes in mixed refrigerants 0.25 R-152a/0.75 R-245fa

Fig. 6 (a) presents the falling film data of 0.25 R-152a/0.75 R-245fa under evaporation temperatures of 20°C and 25°C and flow rate of 240 mL·min⁻¹. The heat transfer coefficient at a saturation temperature of 25°C is higher than that at 20°C. Fig. 6 (b) compares the heat transfer effect of falling film evaporation and pool boiling. The heat transfer coefficient of pool boiling is smaller than falling film evaporation, and the heat transfer trend is similar.



(a) falling film of top tube and center tube



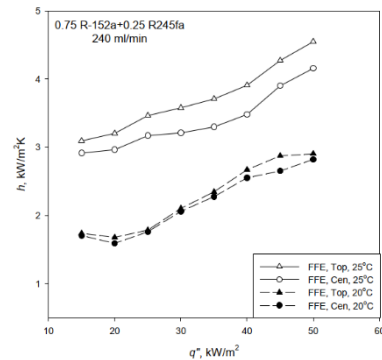
(b) overall

Fig. 6 (a), (b) Mixed Refrigerants (0.25 R-152a / 0.75

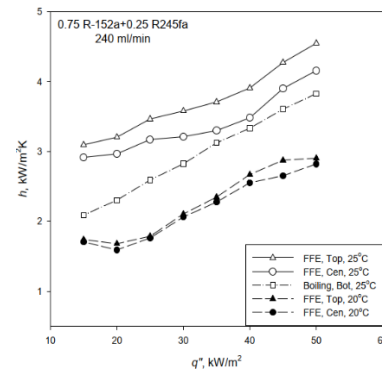
R-245fa): Comprehensive comparison of heat transfer under different temperatures in the plain tubes.

Falling film on plain tubes in mixed refrigerants 0.75 R-152a/0.25 R-245fa

Fig. 7 (a) presents the falling film data of 0.75 R-152a/0.25 R-245fa under evaporation temperatures of 20°C and 25°C and a flow rate of 240 mL·min⁻¹. The heat transfer coefficient at a saturation temperature of 25°C is higher than that at 20°C. However, the differences in heat transfer caused by the different temperatures were between 7.14% and 16.6%. This may be because the difference between the physical properties of mixed and pure refrigerants was small under this blending ratio. Fig. 7 (b) compares pool boiling and falling film evaporation under different saturation temperatures. The results indicated that the trends of heat transfer coefficients of falling film evaporation and pool boiling were similar at 25°C. The heat transfer coefficient of falling film evaporation at 25°C are greater than that at 20°C at the same heat flux.



(a) falling film of top tube and center tube



(b) overall

Fig. 7 (a), (b) Mixed Refrigerants (0.75 R-152a / 0.25 R-245fa): Comprehensive comparison of heat transfer under different temperatures in the plain tubes.

Comparison of R-152 and R-245fa and mixing refrigerants in falling film vaporization

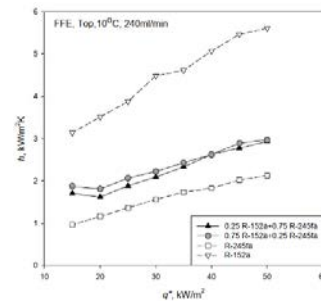
Fig. 8 (a) and (b) present the amount of heat transferred in falling film evaporation of the four different refrigerants at 10°C as well as compare the

heat transfer of the top and center tubes. The findings showed that R-152a had the greatest heat transfer followed by the mixed refrigerants, and R-245fa had the lowest. Judging from the physical properties of the refrigerants, the surface tension directly affected the refrigerant wettability on the tube surface. The surface tension was ranked in ascending order as follows: R-152a, the mixed refrigerants, and R-245fa.

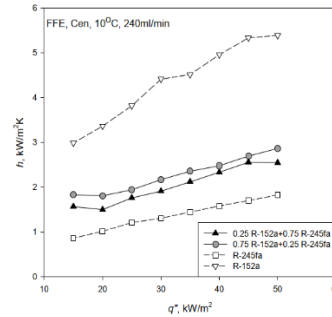
According to the falling film evaporation heat transfer characteristics in Fig. 8 (a) and (b), the heat transfer performance of the two mixtures having the R-152a/R-245fa ratios of either 0.75/0.25, or 0.25/0.75 was higher than that of pure R-245fa. The more volatile fluid R-152a helped improving the heat transfer performance of R-245fa. Furthermore, the heat transfer of the top and center tubes increased by 0.3–0.4 and 0.11–0.131 times, respectively.

According to the comparison of heat transfer in the range 50–20 kW·m⁻² in Fig. 6 (b) and Fig. 7 (b), the heat transfer coefficient of the 0.25/0.75 mixed refrigerants was in the range of 3.0–1.5 kW·m⁻²K⁻¹ at high heat fluxes, and 0.8–1.8 kW·m⁻²K⁻¹ at low heat fluxes. For the 0.75/0.25 mixed refrigerants, the heat transfer coefficient varied from 3.0–2.2 kW·m⁻²K⁻¹ at high heat fluxes to 1.1–1.8 kW·m⁻²K⁻¹ at low heat fluxes. The heat transfer distribution band of the R-152/R245fa ratio = 0.25/0.75 mixed refrigerants was wider than that of the 0.75/0.25 mixed refrigerant. A possible reason for this was that the blending ratios caused differences in temperature glide. Moreover, because of the different blending ratios, the vapor region of the mixed refrigerants was thicker, which increased thermal resistance and phase change.

A comparison of the heat transfer properties of R-152a and R-245fa mixtures in Fig. 6 (c) and Fig. 7 (c) with those of the pure refrigerants in Fig. 5 (c) and Fig. 6 (c) revealed that the heat transfer performance of the pure refrigerants was higher at a saturation temperature of 20°C than at 10°C. However, the heat transfer performances of pure R-152a and pure R-245fa were higher at a saturation temperature of 10°C than at 20°C. This could be because dephlegmation, produced during the evaporation process of zeotropic mixtures, formed two fluids, one of which was suppressed by another refrigerant during the evaporation process. Furthermore, the suppression was greater when the temperature was higher, causing the heat transfer performance to be less satisfactory at higher temperatures than at lower temperatures. Furthermore, this showed that the zeotropic mixtures had individual physical properties that affected the heat transfer performance.



(a) falling film of top tube



(b) falling film of center tube

Fig. 8 (a), (b) R-152a / R-245fa with blending ratios of 0.25/0.75 and 0.75/0.25 Comparison of heat transfer at 10°C and 240 mL/min.

Characteristics of mixed refrigerants

Disjointed dew points and bubble curves in zeotropics cause inconsistent boiling points. The application of zeotropics in the evaporation and condensation processes generates mass transport phenomena because of a phase change in the refrigerant, which affects the heat transfer coefficient. Because of the compositional characteristics of zeotropics, their heat transfer performance is complicated and difficult to predict.

The NIST REFPROP 10.0 commercial software (Lemmon et al. (2018)) was used to analyze the refrigerants’ properties. The results revealed that the blending ratio of zeotropics could affect the heat transfer performance. However, the distribution range was limited. The zeotropics may still have been affected by the characteristics of individual refrigerants, and thus, the evaporation and condensation rates were inconsistent, indicating temperature glide. Temperature glide is a phenomenon where different corresponding pressures are present under the same temperature. At the same pressure, the concentration ratio of a saturated vapor or liquid when it evaporates will be different to when it condenses. As a result, the physical properties of zeotropics fell between the two refrigerants, improving the performance compared with the other refrigerants.

The factors affecting the evaporation rate of refrigerants are their density, the saturation pressure, the flow rate of liquid refrigerants, the boiling temperature, and the concentration of vaporized refrigerants. In the mixed refrigerants, the evaporation

rate of R-152a was $0.0778 \text{ g}\cdot\text{cm}^{-2}\cdot\text{s}^{-1}$, which was $0.023 \text{ g}\cdot\text{cm}^{-2}\cdot\text{s}^{-1}$ higher than the R-245fa. This revealed that the main heat transfer was dominated by R-152a (i.e., the refrigerants with a lower boiling point).

After mixing and under the same temperature and pressure, the saturation pressure of the 0.25/0.75 refrigerants was 25.832 psia, which was higher than the 9.656 psia of R-245fa but lower than the 45.655 psia of R-152a. R-245fa evaporated easily, and overall, the amount of R-152a that evaporated was larger than that of R-245fa; thus, the heat transfer performance of this mixed refrigerants fell between the two separate refrigerants.

The vapor concentration of each component in the mixed vapors affected the vapor diffusion ability. According to Raoult's law, the mixed vapor pressure (p) is equal to the sum of the products of the molar fractions (x_A) of each composition and vapor pressure of the pure refrigerant (p_A^*), as shown in Eq. (10).

$$p = p_A^*x_A + p_B^*x_B + \dots \quad (10)$$

The molar ratio of R-152/R-245fa (0.25/0.75) was calculated using Eq. (10), where the molar concentrations were 0.141 and 0.858, respectively. The saturated vapor pressure of the mixed refrigerants was analyzed with the mass ratio of R-152a/R-245fa (0.25/0.75) and converted to respective volumes of 0.316 L and 0.646 L.

Because of the difference in blending ratios, the refrigerants vapor composition in the chamber differed. When the blending ratio of the refrigerants R-152a/R-245fa was 0.25 / 0.75, the vapor molar concentrations of R-152a and R-245fa were 0.141 and 0.858, respectively. This indicated that under the same volume, the concentration of R-245fa was higher than that of R-152a, which suppressed the evaporation efficiency of R-152a.

According to Graham's law, the diffusion rate is related to vapor density. Under the blending ratio of 0.25/0.75, the diffusion rate of R-245fa (0.5) was higher than that of R-152a (0.318), and thus the diffusion ability of R-152a was suppressed. Because the respective refrigerant R-245fa was already undergoing heat exchange for latent heat when R-152a remained in a liquid state, the main heat transfer mechanism was dominated by R-245fa. This could be observed from the falling film of heat transfer curve, the trend of which was closer to R-245fa.

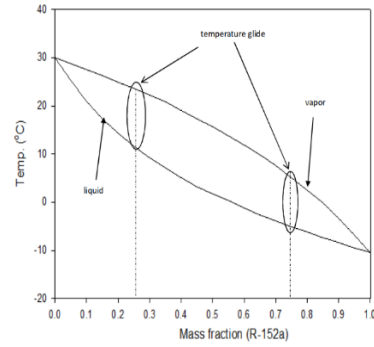


Fig. 9 Temperature glide of R-152a and R-245fa for 0.212 MPa

Fig. 9 shows the boiling/dew point temperature-composition chart of R-152a/R-245fa mixture at 0.212 MPa, generated by the NIST REFPROP 10.0 commercial software. As shown in Fig. 9, a comparison of bubble and dew point temperatures of the 0.25/0.75 and 0.75/0.25, R-152a/R-245fa mixed refrigerant revealed that the temperature glide of the 0.75/0.25 refrigerant was smaller than that of the 0.25/0.75 one. A large temperature glide indicated that the heat transfer performance distribution band of the entire falling film evaporation process was wider; otherwise, it was narrower. Therefore, temperature glide is closely related to heat transfer. Changing the blending ratio of zeotropics affects the difference between the bubble and dew point temperature and the heat transfer performance. In this experiment, the 0.25/0.75 refrigerant exhibited a larger heat transfer range than did the 0.75 / 0.25 refrigerant.

According to Fig. 9, when the R-152a/R-245fa mixed refrigerants was in a ratio of 0.25 / 0.75, the temperature glide had a larger difference, which affected the heat transfer performance. Fig. 9 could explain that binary refrigerant heat transfer performance curve is related to non-linearity.

The temperature glide of the zeotropics differed because of the different boiling points. The differences in bubble and dew point temperatures differed under the various blending ratios, making the heat transfer performance difficult to predict. Eq.(11) and (12) were developed by Dang et al.(2018) using the known mass concentration (ϕ) of the volatile component and experimental data of wall superheats (ΔT_1 and ΔT_2) of each pure refrigerant to calculate the difference between actual and predicted heat transfer values of the mixed refrigerants.

$$\Delta T_{id,sup} = \phi \Delta T_1 + (1 - \phi) \Delta T_2 \quad (11)$$

$$h_{id,b} = \frac{q}{\Delta T_{id}} = \left[\phi \left(\frac{q}{\Delta T_1} \right)^{-1} + (1 - \phi) \left(\frac{q}{\Delta T_2} \right)^{-1} \right]^{-1} \quad (12)$$

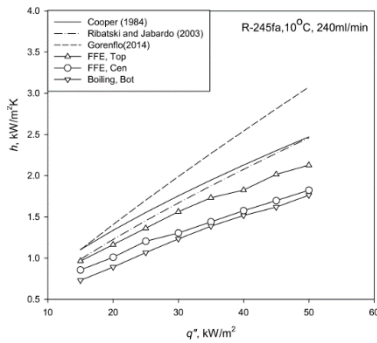
Fig. 10 (a) and (b) compare the empirical formulas of this study with those of Cooper.(1984), Ribatski and Jabardo (2003), and Gorenflo et al.(2014) for R-245fa at saturation temperatures of 10°C and

20°C. The results showed that the predicted data at 20°C of Ribatski and Jabardo correlation were closer to the experimental data of the present study, whereas the deviation was larger at 10°C. In addition, Fig. 10 (c) and (d) compare the data of this study with the prediction of Cooper, Ribatski and Jabardo, Gorenflo for R-152a at saturation temperatures of 10°C and 20°C. The results revealed that the predicted data at 10°C of Ribatski and Jabardo were closer to the experimental data of the present study, whereas the deviation was larger at 20°C. The results of this experiment showed that the trend of predicted values was consistent with the aforementioned studies, where the predicted values of Ribatski and Jabardo were the closest to the experimental data of the present study.

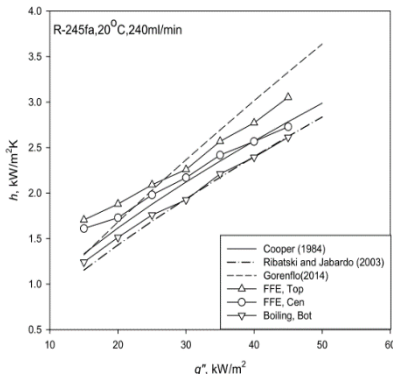
Eq. (13) is an empirical correlation for the heat transfer coefficient of Cooper’s nucleate boiling:

$$h_{nb} = 90 \cdot q''^{0.67} \cdot M^{-0.5} \cdot P_{red}^m \cdot (-\log_{10} P_{red})^{-0.55} \quad (13)$$

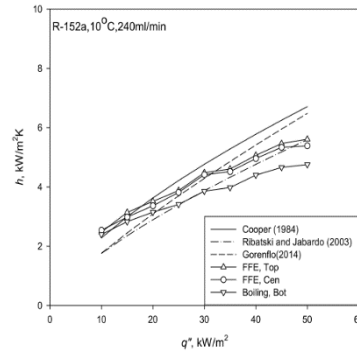
where $m = 0.12 - 0.2 \cdot \log_{10} R_p$; q'' is heat flux; M is the molecular weight of the working fluid; P_{red} is the reduced pressure; and R_p is surface roughness. This R_p is 0.1 μm .



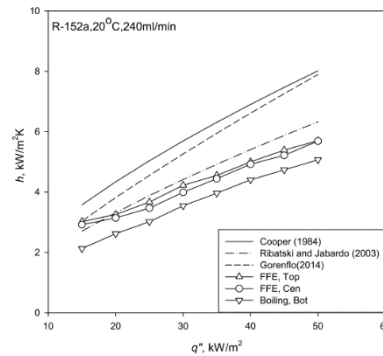
(a) Comparison of the 10°C experiment in this study with that of Ribatski, Gorenflo, and Cooper for R-245fa



(b) Comparison of the 20°C experiment in this study with that of Ribatski, Gorenflo, and Cooper for R-245fa.



(c) Comparison of the 10°C experiment in this study with that of Ribatski, Gorenflo, and Cooper for R-152a.



(d) Comparison of the 20°C experiment in this study with that of Ribatski, Gorenflo, and Cooper for R-152a.

Fig. 10 (a), (b), (c), and (d) R-152a: Comparison of this study’s experimental data with those of Ribatski, Gorenflo, and Cooper for R-152a and R-245fa. ($R_p=0.1 \mu m$.)

Eq. (14) is the empirical correlation for the heat transfer coefficient of Ribatski and Jabardo’s nucleate boiling:

$$h_{nb} = 100 \times q''_{wall} P_{red}^{0.45} [-\log P_{red}]^{-0.8} R_p^{0.2} M^{-0.5} \quad (14)$$

where $n = 0.9 - 0.3 P_{red}^{0.2}$,

Eq. (15) is the empirical correlation for the heat transfer coefficient of Gorenflo’s nucleate boiling:

$$h_{nb} = 3580 \cdot F_q \cdot F_{P_{red}} \cdot F_f \cdot F_w \quad (15)$$

where $F_q = (q'' / q_0'')^{n(P_{red})}$, $q_0'' = 20000 kW / m^2$,

$$n(P_{red}) = 0.95 - 0.3 P_{red}^{0.3}$$

$$F_{P_{red}} = 0.7 P_{red}^{0.2} + 4 P_{red} + [1.4 P_{red} / (1 - P_{red})]$$

$$F_f = [(P_f / P_{f,ref})^{0.6}]_{P_{red}=0.1}, \text{ when the reduced pressure is 0.1}$$

of the pressure slope.

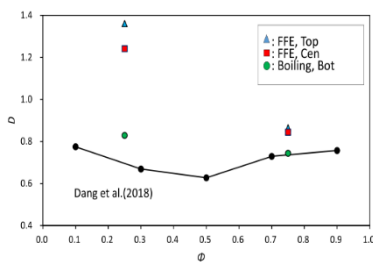
$$F_w = (R_p / R_{po})^{2/15} [(\lambda \rho c)_w / (\lambda \rho c)_{cu}]^{1/4}, \quad R_{po} = 0.4 \mu m$$

When the zeotropic mixture was under the same dew and bubble point temperatures, the concentrations of the components may change because of the different

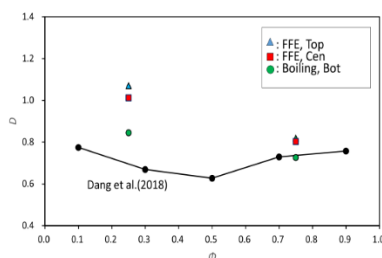
boiling points of the individual refrigerants, which may have affected the heat transfer performance. To demonstrate the performance degradation during heat transfer, Dang et al.(2018) used Eq. (16) to define the degradation factor (D), where h_b represents the actual boiling heat transfer and $h_{id,b}$ represents the ideal boiling heat transfer, given by Eq. (12), where ϕ is the mass concentration of R152a .

$$D = \frac{h_b}{h_{id,b}} \quad (16)$$

The values of D were reduced from the present experimental data, and compared with those of Dang et al. (2017) in Fig. 11 (a) and (b) at 10°C and 20°C system temperatures, respectively. For both 10°C and 20°C, the D values of boiling on the bottom tube in the present tests of R-152a/R-245fa mixture at $\phi=0.75$ are very close to the value of R-134a/R-245fa mixture in Dang et al. (2017). The boiling heat transfer coefficient of pure R-152a is greater than that of pure R-134a as found by Pan (2014). The D values of present boiling tests at $\phi=0.25$ is 0.83, which is slightly higher than those (0.67~0.77) of R-134a/R-245fa mixtures in Dang et al. (2017) because the more volatile component, R-152a, contributes a higher heat transfer coefficient. However, the D values of falling film evaporation on top and center tubes are significantly higher than that of boiling on the bottom tube. For 0.25 mass fraction, the D values of falling film evaporation are even greater than one, which indicates an enhancement of heat transfer by the mixture as compared with their pure components. This indicates that the falling film evaporative heat transfer coefficient is greater than the ideal value, predicted by Eq. (12), contributed by each component with 0.25 concentration of R-152a. This may be because that the more volatile fluid can evaporate more efficiently with the assist of the less volatile fluid by forming a layer of liquid film.



(a) Comparison of the mixed refrigerants at 10°C in this study with those of Dang et al.



(b) Comparison of the mixed refrigerants at 20°C of this study with those of Dang et al.

this study with those of Dang et al.

Fig. 11 (a) and (b) Comparison of the mixed refrigerants of this study with those of Dang et al.

CONCLUSION

This study drew the following conclusions.

1. For the zeotropic mixed refrigerants R-152a/R-245fa with blending ratios of 0.75/0.25 and 0.25/0.75, the heat transfer coefficients are smaller than those of R-152a but larger than those of R-245fa.
2. For the zeotropic mixed refrigerants R-152a/R-245fa at a ratio of 0.25/0.75, the heat transfer band was wider than that of the 0.75/0.25 blend. However, the heat transfer characteristics presented a flatter heat transfer curve from 50–20 kW m⁻²K⁻¹, and furthermore, the heat transfer coefficient spanned a wider range.
3. When the heat flux was < 20 kW m⁻², the zeotropic mixed refrigerants tended to have the lowest falling film evaporation point where the heat flux decreased and heat transfer increased.

Changing the blending ratio affected the temperature glide, which further altered the heat transfer performance. The degradation factor of falling film evaporation is greater than that of boiling. Instead of performance degradation, the falling film evaporative heat transfer of the R-152a/R-245fa mixture is greater than the ideal value at 0.25 mass concentration of R-152a.

ACKNOWLEDGEMENTS

We thank the Ministry of Science and Technology, Taiwan, for financial support (MOST 108-3116-F-027-001).

REFERENCES

- Chang, T. B. and Chiou, J. S., “Spray evaporation heat transfer of R-141b on a horizontal tube bundle,” *International Journal of Heat and Mass Transfer*, Vol. 42, pp. 1467-1478 (1999).
- Chien, L.-H., Tsai Y. and Chang, C., A study of pool boiling and falling-film vaporization with R-245fa/oil mixtures on horizontal tubes, *International Journal of Heat and Mass Transfer*, Vol. 133, pp. 940–950, (2019).
- Chien*, L-H. and Chen, R-H., “An experimental study of falling film evaporation on horizontal tubes using R-134A,” Vol. 28, No. 2, (2012).
- Chien, L-H. and Cheng, H-C., “A predictive model of falling film evaporation with bubble nucleation on horizontal tubes,” *International Journal of HVAC&R Research*, Vol. 12, pp. 69-87 (2006).
- Chien, Liang-Han. and Tsai, Yue-Lin., “An experimental study of pool boiling and falling film vaporization on horizontal tubes in R-

- 245fa," pp. 4044-4054 (2011).
- Cooper, M. G., "Saturation nucleate pool boiling – a simple correlation," *International Chemical Engineering Symposium Series*, Vol. 86, pp. 785-793 (1984).
- Dang, C., Jia, L., Peng, Q., Huang, Q. and Zhang, X., "Experimental and analytical study on nucleate pool boiling heat transfer of R134a/R245fa zeotropic mixtures," *International Journal of Heat and Mass Transfer*, Vol. 119, pp. 508–522 (2018).
- Dang, C., Jia, L., Xu, M., Huang, Q., Peng, Q., "Experimental study on flow boiling characteristics of pure refrigerant (R134a) and zeotropic mixture (R407C) in a rectangular micro-channel," *Int. J. Heat Mass Transfer*, Vol. 104, pp. 351–361 (2017).
- Fernández-Seara, J. and Pardiñas, Á.Á., "Refrigerant falling film evaporation review: description, fluid dynamics and heat transfer," *Appl. Therm. Eng.*, Vol. 64, pp. 155–171 (2014).
- Fujita, Y. and Tsutsui, M., "Experimental investigation of falling film evaporation on horizontal tubes," *Heat Transfer-Japanese Research*, Vol. 27, pp. 609-618 (1998).
- Fujita, Y., Tsutsui, M. and Zhou, Z-Z., "Evaporation heat transfer of falling films on horizontal tube - part 1, analytical study," *Heat Transfer-Japanese Research*, Vol. 24, pp. 1-16 (1995).
- Fujita, Y., Tsutsui, M. and Zhou, Z-Z., "Evaporation heat transfer of falling films on horizontal tube - part 2, experimental study," *Heat Transfer-Japanese Research*, Vol. 24, pp. 17-31 (1995).
- Gorenflo*, D., Baumhögger, E., Herres, G., and Kotthoff, S., "Prediction methods for pool boiling heat transfer: A state-of-the-art review," *International Journal of Refrigeration*, Vol 43, pp. 203-226 (2014).
- Ji, W. T., Zhao, C. Y., Zhang, D. C., Yoshika, S., He, Y. L., and Tao, W. Q., "Effect of vapor flow on the falling film evaporation of R134a outside a horizontal tube bundle," *International Journal of Heat and Mass Transfer*, Vol. 92, pp. 1171–1181 (2016).
- Ji, W. T., Zhao, E., Zhao, C., Zhang, H., and Tao, W., "Falling film evaporation and nucleate pool boiling heat transfer of R134a on the same enhanced tube," *Applied Thermal Engineering*, Vol. 147, pp. 113–121 (2019).
- Jin, P., Zhang, Z., Mostafa, I., Zhao, C. Ji, W., and Tao, W., "Heat transfer correlations of refrigerant falling film evaporation on a single horizontal smooth tube," *International Journal of Heat and Mass Transfer*, Vol. 133, pp. 96–106 (2019).
- Jung, D., Song, K., Ahn, K. and Kim, J., "Nucleate boiling heat transfer coefficients of mixtures containing HFC32, HFC125, and HFC134a," *Int. J. Refrig.*, Vol. 26, pp. 764–771 (2003).
- Lemmon, E. W., Bell, I. H., Huber, M. L. and McLinden, M. O., NIST standard reference database 23: Reference Fluid Thermodynamic and Transport Properties Database (REFPROP): version 10.0, National Institute of Standards and Technology, Standard Reference Data Program, Gaithersburg (2018).
- Moeykens, S. and Pate, M. B., "Effect of lubricant on spray evaporation heat transfer performance of R-134a and R-22 in tube bundles," *ASHRAE Transactions*, Vol. 102, No. 1, pp. 410-426 (1996).
- Moeykens, S. and Pate, M. B., "Spray evaporation heat transfer performance of R- 134a on plain tubes," *ASHRAE Transactions*, Vol. 100, No. 2, pp. 173-184 (1994).
- Moeykens, S. and Pate, M. B., "The effects of nozzle height and orifice size on spray evaporation heat transfer performance for a low-finned. triangular-pitch tube bundles with R-134a," *ASHRAE Transactions*, Vol. 101, No. 2, pp. 420-433 (1995).
- Moeykens, S., Kelly, J. E. and Pate, M. B., "Spray evaporation heat transfer performance of R-123 in tube bundles," *ASHRAE Transactions*, Vol. 102, No. 2, pp. 259-272 (1996).
- Moeykens, S., Newton, B. J. and Pate, M. B., "Effects of surface enhancement. film-feed supply rate. and bundle geometry on spray evaporation heat transfer performance," *ASHRAE Transactions*, Vol. 101, No. 2, pp. 408-419 (1995).
- Pan, C.-H., "A Heat Transfer Study of Falling Film Evaporator using R-152a, master thesis, National Taipei University of Technology." (2014)
- Ribatski, G. and Jacobi, A. M., "Falling film evaporation on horizontal tubes - a critical review," *International Journal of Refrigeration*, Vol. 28, No. 5, pp. 635-653 (2005).
- Ribatski, G. and Jabardo, J. M. S., "Experimental study of nucleate boiling of halocarbon Refrigerants on cylindrical surfaces," *International Journal of Heat and Mass Transfer*, Vol. 46, pp. 4439–4451 (2003),.
- Roques, J. F. and Thome, J. R. "Falling films on arrays of horizontal tubes with R-134a, part II: flow visualization. onset of dryout, and heat transfer predictions," *Heat Transfer Engineering*, Vol. 28, pp. 415-434 (2007).
- Sarbu, I., "A review on substitution strategy of non-ecological refrigerants from vapour compression-based refrigeration, air-conditioning and heat pump systems," *Int. J. Refrig.*, Vol. 46, pp. 123–141 (2014).
- Stralen, S. J. D. V. and Sluyter, W. M., "Investigations on the critical heat flux of pure liquids and mixtures under various conditions," *Int. J. Heat Mass Transf.*, Vol. 12, pp. 1353–1384 (1969).
- Stralen, S. J. D. V., "The boiling paradox in binary

- liquid mixtures," Chem. Eng. Sci., Vol. 25, pp. 149–171 (1970).
- The Montreal Protocol on Substances that Deplete the Ozone Layer, ISBN: 92-807-1888-6
- Zhao, C. Y., Ji, W. T., and Jin, P. H., "Cross vapor stream effect on falling film evaporation in horizontal tube bundle using R134a," Heat Transfer Eng., Vol. 38, pp. 1–14 (2017).
- Zhao, C. Y., Ji, W. T., and Jin, P. H., "Experimental study of the local and average falling film evaporation coefficients in a horizontal enhanced tube bundle using R134a," Appl. Therm. Eng., Vol. 129, pp. 502–511 (2018).

NOMENCLATURE

- A_t total surface area of evaporation (m^2)
- C_p specific heat constant for a fixed pressure ($kJ \cdot mol^{-1} \cdot K^{-1}$)
- d tube diameter (m)
- D $h_b/h_{id,b}$
- F_p install level pitch of test tube (mm)
- G mass velocity ($kg \cdot m^{-2} \cdot s$)
- g acceleration due to gravity ($m \cdot s^{-2}$)
- h heat transfer coefficient ($W \cdot m^{-2} \cdot K^{-1}$)
- h_{fg} latent heat of evaporation ($kJ \cdot kg^{-1}$)
- h_{nb} nucleate boiling heat transfer coefficient ($W \cdot m^{-2} \cdot K^{-1}$)
- h_{pred} heat transfer coefficient predicted by the new model
- k thermal conductivity ($W \cdot m^{-1} \cdot K^{-1}$)
- L_h heating length (m)
- M molecular weight
- \dot{m} mass flow rate ($kg \cdot s^{-1}$)
- Nu Nusselt number
- P_{red} reduced pressure
- P_s system pressure
- Pr_f liquid Prandtl number
- q'' heat flux ($W \cdot m^{-2}$)
- R_p surface roughness (μm)
- r tube radius (m)
- Re_f film Reynolds number
- S_{spr} correction factor of nucleate boiling in falling film
- T temperature ($^{\circ}C$)
- T_p Interval of Test Tube (mm)
- v_g specific volume of vapor ($m^3 \cdot kg^{-1}$)
- φ Mixture ratio

Greek Symbol

- ΔT_{ws} wall superheat (K)
- α thermal diffusivity ($m^2 \cdot s^{-1}$)
- δ film thickness (m)
- ρ density ($kg \cdot m^{-3}$)
- σ surface tension ($N \cdot m^{-1}$)
- μ dynamic viscosity (Pa s)
- ν kinematic viscosity ($m^2 \cdot s^{-2}$)

Γ mass flow rate per unit length ($kg \cdot s^{-1} \cdot m^{-1}$)

Subscript

- cv Convective
- exp Experimental
- f Liquid
- i Inside
- in Inlet
- m Mean
- nb nucleate boiling
- o Outside
- pred Predicted
- s Saturated
- w tube wall

非共沸混合冷媒在光滑管的滴淋熱傳分析

張景閔 簡良翰

國立台北科技大學 能源與冷凍空調工程系

摘要

本研究以 R-152a 和 R-245fa 冷媒以不同的混合比及飽和溫度下做滴淋蒸發熱傳研究。研究 R-152a / R-245fa 混合冷媒在 0.75 / 0.25 和 0.25 / 0.75 的混合比下的熱傳性能。對於滴淋蒸發，以光滑管水平放置在飽和溫度為 10 $^{\circ}C$ 和 20 $^{\circ}C$ 的測試腔體內。測試結果表明熱傳性能變化與冷媒的混合比例不成線性比例關係。R-152 / R-245fa 混合比 = 0.25 / 0.75 的混合冷媒的熱傳分佈帶比 0.75 / 0.25 混合比的冷媒的熱傳分佈帶為寬。造成這種情況的可能原因是混合比例導致了溫度滑移的差異。混合冷媒的熱傳性能高於 R-245fa 冷媒。上管的熱傳有效增加 0.39 - 0.55，中管的熱傳有效增加 0.57 - 0.78。兩種混合冷媒的沸騰熱傳性能均小於由 R-152a 和 R-245fa 的沸騰曲線計算得出的理想熱傳係數。R-152a / R-245fa 混合冷媒的滴淋蒸發熱傳不但沒有降低性能，而且大於在 R-152a 的質量濃度為 0.25 時的理想值。